ADVANCES IN ATMOSPHERIC SCIENCES, VOL. 35, OCTOBER 2018, 1217–1230

• **Original Paper** •

Value-added Impact of Geostationary Hyperspectral Infrared Sounders on Local Severe Storm Forecasts—via a Quick Regional OSSE

Zhenglong LI[1], Jun LI*[1], Pei WANG[1], Agnes LIM[1], Jinlong LI[1], Timothy J. SCHMIT[2], Robert ATLAS[3], Sid-Ahmed BOUKABARA[4], and Ross N. HOFFMAN[3]

[1]*Cooperative Institute for Meteorological Satellite Studies, University of Wisconsin-Madison, 1225 West Dayton Street, Madison, WI* 53706*, USA*

[2]*Center for Satellite Applications and Research, NOAA, Madison, WI* 53706*, USA*

[3]*Atlantic Oceanographic and Meteorological Laboratory, OAR/NOAA, Miami, FL* 33149*, USA*

[4]*Center for Satellite Applications and Research, NOAA, College Park, MD* 20740*, USA*

(Received 7 February 2018; revised 27 April 2018; accepted 11 June 2018)

ABSTRACT

Accurate atmospheric temperature and moisture information with high temporal/spatial resolutions are two of the key parameters needed in regional numerical weather prediction (NWP) models to reliably predict high-impact weather events such as local severe storms (LSSs). High spectral resolution or hyperspectral infrared (HIR) sounders from geostationary orbit (GEO) provide an unprecedented source of near time-continuous, three-dimensional information on the dynamic and thermodynamic atmospheric fields—an important benefit for nowcasting and NWP-based forecasting. In order to demonstrate the value of GEO HIR sounder radiances on LSS forecasts, a quick regional OSSE (Observing System Simulation Experiment) framework has been developed, including high-resolution nature run generation, synthetic observation simulation and validation, and impact study on LSS forecasts. Results show that, on top of the existing LEO (low earth orbit) sounders, a GEO HIR sounder may provide value-added impact [a reduction of 3.56% in normalized root-mean-square difference (RMSD)] on LSS forecasts due to large spatial coverage and high temporal resolution, even though the data are assimilated every 6 h with a thinning of 60 km. Additionally, more frequent assimilations and smaller thinning distances allow more observations to be assimilated, and may further increase the positive impact from a GEO HIR sounder. On the other hand, with denser and more frequent observations assimilated, it becomes more difficult to handle the spatial error correlation in observations and gravity waves due to the limitations of current assimilation and forecast systems (such as a static background error covariance). The peak reduction of 4.6% in normalized RMSD is found when observations are assimilated every 3 h with a thinning distance of 30 km.

Key words: OSSE, hyperspectral, sounder, high-impact weather

Citation: Li, Z. L., and Coauthors, 2018: Value-added impact of geostationary hyperspectral infrared sounders on local severe storm forecasts—via a quick regional OSSE. *Adv. Atmos. Sci.*, **35**(10), 1217–1230, https://doi.org/10.1007/s00376-018-8036-3.

1. Introduction

High spectral, or hyperspectral, resolution instruments like the advanced infrared (IR) sounders (Menzel et al., 2018) onboard the low earth orbit (LEO) satellites, such as the Atmospheric InfraRed Sounder (AIRS) (Chahine et al., 2006), Infrared Atmospheric Sounding Interferometer (IASI) (Hilton et al., 2012), and Crosstrack Infrared Sounder (CrIS) (Gambacorta et al., 2014), are able to provide global atmospheric temperature and moisture profile information with high vertical resolution for numerical weather prediction (NWP) models. According to reports from a number of global NWP centers, hyperspectral IR sounders have the largest positive impact, from a single instrument, to the assimilation and prediction results of current operational assimilation forecast systems (Cardinali, 2009; Joo et al., 2013; Mallick et al., 2017). In combination with advanced microwave sounder data, advanced IR sounder data have been successfully assimilated with significant positive impacts at many operational NWP centers. These include the European Centre for Medium-Range Weather Forecasts (McNally et al., 2006; Collard and McNally, 2009; McNally et al., 2014), the National Centers for Environmental Prediction (Le Marshall et al., 2005, 2006a, 2006b), Météo-France (Auligné et al., 2003), and the United Kingdom Met Office (Hilton et al.,

* Corresponding author: Jun LI
Email: jun.li@ssec.wisc.edu

2009).

Monitoring moisture that has large spatial and temporal variability needs more frequent observations. Such high temporal resolution (1 h or better) atmospheric observation can be provided by geostationary satellites, such as the current geostationary operational environmental satellite (GOES) Sounder (Menzel et al., 1998) and advanced imagers. The imagers include the Advanced Baseline Imager (Schmit et al., 2005, 2017) onboard GOES-16 and -S, -T and -U; the Advanced Himawari Imager onboard the Japanese Himawari-8/-9 satellites (Bessho et al., 2016; Ma et al., 2017); and the Advanced Geosynchronous Radiation Imager onboard the Chinese FengYun-4 (FY-4) series (Yang et al., 2017). Those sensors usually lack vertical resolution due to broader spectral response functions (SRFs) and limited channels. On the other hand, high spectral resolution sensors have a much greater vertical resolving power for temperature, moisture, winds and trace gases than low spectral resolution sensors.

A hyperspectral IR sounder onboard a satellite at geostationary orbit can provide four-dimensional atmospheric temperature, moisture, and wind profiles. Schmit et al. (2009) outlined the advantages of a geostationary satellite–based advanced IR sounder on nowcasting, forecasting and NWP applications over a polar orbit satellite–based sounder by providing rapid refresh measurements for severe weather events. An advanced IR sounder called InfraRed Sounder has been planned for the EUMETSAT Meteosat Third Generation sounding mission to be launched in 2022. The Geostationary Interferometric InfraRed Sounder onboard the Chinese FY-4 series (Yang et al., 2017) is the first geostationary satellite–based high spectral resolution IR sounder. Launched on 11 December 2016, FY-4A is the first satellite of the FY-4 series, though it is experimental. Although the Hyperspectral Environmental Suite was removed from the GOES-R series, NOAA continues to have valid justification for measurements from an advanced IR sounder in geostationary orbit (Schmit et al., 2009). In order to understand the unique value of a geostationary advanced IR sounder for high-impact weather (HIW), such as local severe storms (LSSs), a quick regional Observing System Simulation Experiment (rOSSEs) framework has been developed. This includes generating the Nature Run (NR), simulating LEO orbits, simulating and validating the synthetic radiances, impact study of data assimilation, and NWP forecasting of HIW events.

An OSSE, a type of sensitivity experiment, can answer questions related to the value of new or proposed observing systems and how these and other data are assimilated (Atlas, 1997; Atlas et al., 2015; Hoffman and Atlas, 2016). In an OSSE, the NR is very important as a proxy of reality. It should be a free run of a forecast model without observation data assimilation, have realistic phenomenology and variability compared with nature, and should be as independent as possible from the data assimilation system model. With NR data, the new and existing observing systems data can be simulated for assimilation. For a more comprehensive description and explanation of OSSEs, see Hoffman and Atlas (2016). OSSEs are classified into two categories depending on the NR and the forecast model. A global OSSE uses a global NR and global NWP forecast model with a focus on large-scale weather systems. A quick rOSSE uses a high-resolution regional NR (or a global NR if the resolution requirement is met or embedded in the global NR, if possible) and a regional NWP model with a focus on mesoscale or small-scale HIW events, such as LSSs and tropical cyclones.

A global OSSE with a geostationary advanced IR sounder has been developed by NOAA's Joint Center for Satellite Data Assimilation (Boukabara et al., 2016a, 2018), with a focus on global-scale weather systems. The quick rOSSE method has been widely used to understand the value-added impact of future observations, such as the NASA Cyclone Global Navigation Satellite System (Zhang et al., 2017), and geostationary hyperspectral IR sounder (Wang et al., 2013; Jones et al., 2017). In this study, a quick rOSSE is carried out to study the impact of a geostationary advanced IR sounder on HIW forecasts compared with existing LEO sounders, including advanced IR sounders such as AIRS, IASI and CrIS.

In this work, the orbit simulator and radiance simulation/validation are introduced in section 2. The assimilation experiments and impact study are outlined in section 3, followed by a discussion in section 4. Finally, a summary and outlook are given in section 5.

2. Simulation and validation

In rOSSE-based studies, the first step is the simulation, including the NR, the orbits, and the synthetic observations. This section provides details on how the simulations are carried out and how they are validated.

2.1. *NR*

In an OSSE study, the NR represents the real atmospheric state, which requires coverage over a large domain and high spatial and temporal resolutions to provide optimal atmospheric information for both the simulation and assimilation. For an LSS OSSE, a very high resolution NR is needed to capture the mesoscale structures in the storms. For this study, the Weather Research and Forecasting-Nonhydrostatic Mesoscale Model (WRF-NMM), version 3.6.1, is used as the regional NWP model to generate the high-resolution NR (HRNR), with a spatial resolution of 2 km. The domain covers almost the whole of the continental United States and part of the eastern Pacific Ocean, with grid points of 3200 (lon) × 1320 (lat) (see Fig. 1 for the NR domain coverage, along with the imagery of storm relative helicity at 0600 UTC 27 May 2006). The model is set up with 51 vertical layers from the surface to a model top at 10 hPa. The schemes used include the Eta (Ferrier) microphysics scheme, the GFDL longwave and shortwave schemes, the Eta similarity surface layer scheme, the Noah land surface model, and the MYJ planetary boundary layer scheme. No cumulus parameterization is needed due to the high resolution (2 km) of the HRNR (Skamarock and Weisman, 2009).

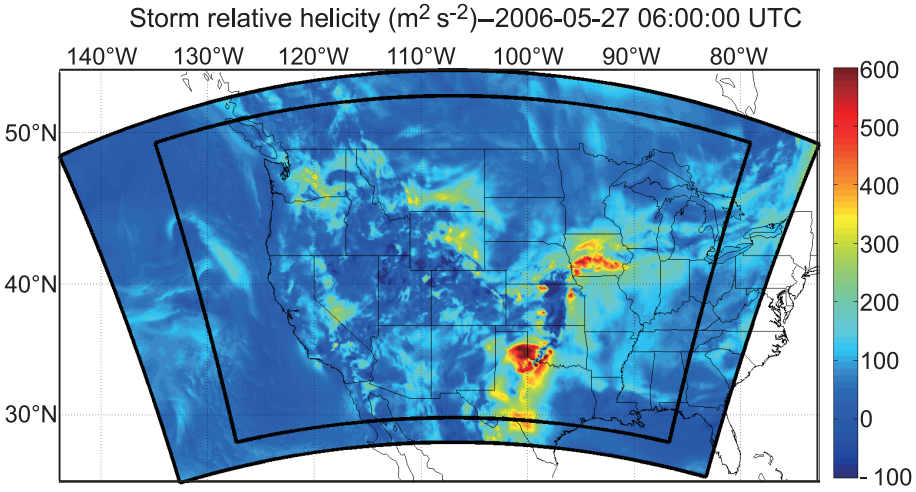

Fig. 1. Model domain for the NR (outer black lines) and experiments (inner black lines). The values shown are storm relative helicity at 0600 UTC 27 May 2006. Note the pattern of storm relative helicity is similar to the accumulated precipitation shown in the bottom panel in Fig. 2.

To avoid the impact of the real atmosphere, the initial and boundary data are from the global OSSE six-hourly Global Forecast System (GFS) analysis (Lim et al., 2017). The global OSSE uses the Goddard Earth Observing System Model Version 5 NR (G5NR, Gelaro et al., 2015). Most existing observation systems are assimilated in the global OSSE, such as the conventional radiosonde observations (RAOBs), surface observations, aircraft, profilers, radiances from AMSU-A onboard the MetOp and NOAA satellites, Advanced Technology Microwave Sounder (ATMS), AIRS, IASI, CrIS, and the GPS radio occultation (GPSRO) bending angle. The global OSSE output files have a $1^\circ \times 1^\circ$ resolution, with 27 vertical levels from the surface to 10 hPa. The original resolutions are downscaled for the HRNR by the WRF model.

The HRNR initializes at 1800 UTC 25 May 2006, and forecasts for 54 h, ending at 0000 UTC 28 May 2006. The storm runs from 0000–1200 UTC 27 May. The HRNR is 30 h ahead of the storm event, to fully prepare the data simulation and assimilation experiments. Figure 2 shows the 3-h precipitation from the HRNR at 0600 UTC 27 May, along with that from the G5NR. The storm precipitation is mainly in southeastern Nebraska, western Iowa, central Kansas and southward to southern Oklahoma and Texas. The HRNR clearly catches the storm precipitation pattern and location as reasonably well as G5NR, but the HRNR has much finer spatial resolution and shows much better spatial structures of the LSS than the G5NR. Due to the high spatial resolution, the precipitation intensity of the HRNR is also stronger than that of the G5NR. Note that the pattern of the accumulated precipitation shown in the upper panel of Fig. 2 is similar to the storm relative helicity shown in Fig. 1.

2.2. *LEO orbit simulator*

A satellite orbit simulator was developed at the University of Wisconsin-Madison to simulate LEO satellite orbital information based on track information (Frederick W. Nagle, personal communication). For given starting and ending times, the simulator calculates the orbital information, such as geolocation, satellite geometry (both zenith and azimuth angle), solar geometry, time, etc. For CrIS and IASI, the field of view (FOV) numbers are also provided. Such information is needed for simulating LEO radiance observations. The simulator has excellent agreement with real observations, as shown in Fig. 3 for CrIS and IASI/MetOp-A for half of the scan line of a randomly selected granule. Besides, the satellite orbit simulator has been expanded to include many other instruments, such as AIRS, IASI/MetOp-B, AMSU-A from the NOAA satellites, Aqua and MetOp-A/B, ATMS, etc. The orbit simulator can also simulate orbits for future sensors as well, like the microwave sensors for TROPICS (Time-Resolved Observations of Precipitation structure and storm Intensity with a Constellation of Smallsats) mission (https://tropics.ll.mit.edu/CMS/tropics/Mission-Overview).

2.3. *Radiative transfer model*

An efficient hyperspectral IR radiative transfer model (HIRTM) has been developed to simulate synthetic radiance observations in both clear and cloudy skies (Li et al., 2017) for AIRS, CrIS and IASI. The HIRTM uses the Stand-alone AIRS Radiative Transfer Algorithm (SARTA; Hannon et al., 1996; Strow et al., 2003) for atmospheric transmittance calculation. The cloud absorption and scattering are calculated using the cloudy model developed by Wei et al. (2004). Figure 4 shows a clear-sky RTM comparison between SARTA and the Community RTM (CRTM) for CrIS. The University of Wisconsin-Madison (UW-Madison) SeeBor database [15 704 global profiles (Seemann et al., 2003, 2008)] are used as inputs in the radiance calculations. The statistical results show that the CRTM [version 2.1.3, with optical depth in pressure space coefficients (Chen et al., 2010, 2012)] agrees with SARTA reasonably well, especially for the window re-

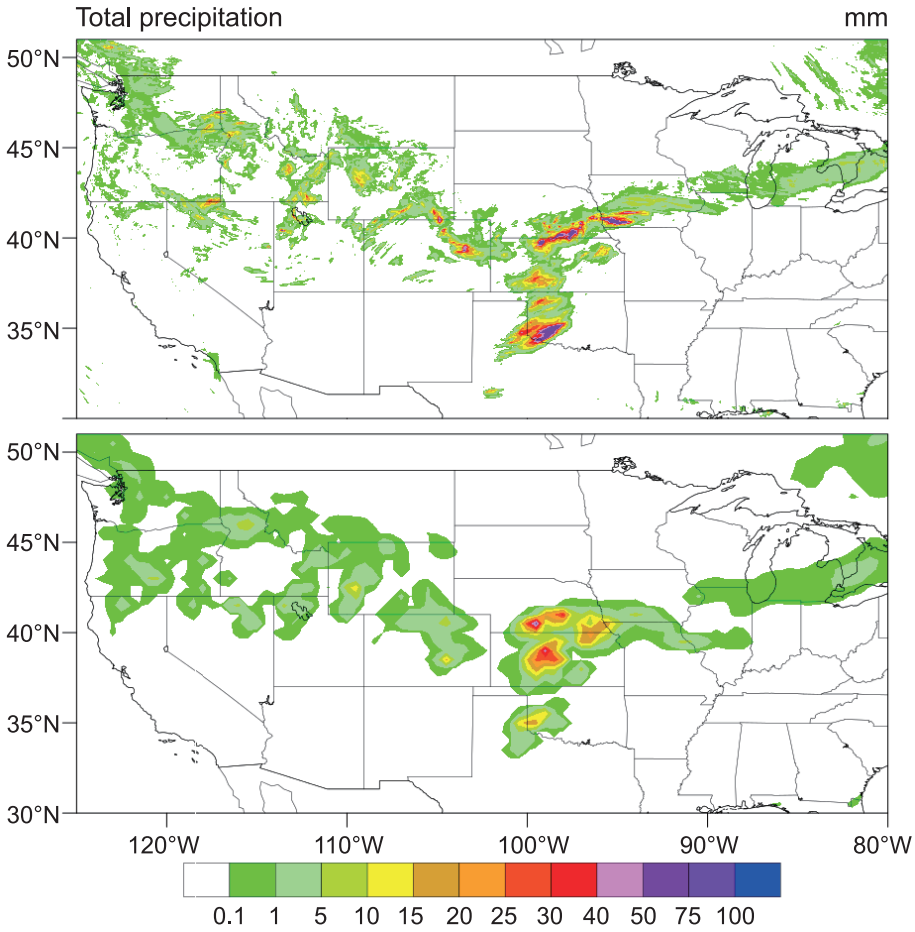

Fig. 2. Three-hour precipitation from HRNR (upper) and G5NR (lower) from 0300–0600 UTC 27 May 2006. Note the pattern of 3-h accumulated precipitation is similar to the storm relative helicity at 0600 UTC shown in Fig. 1.

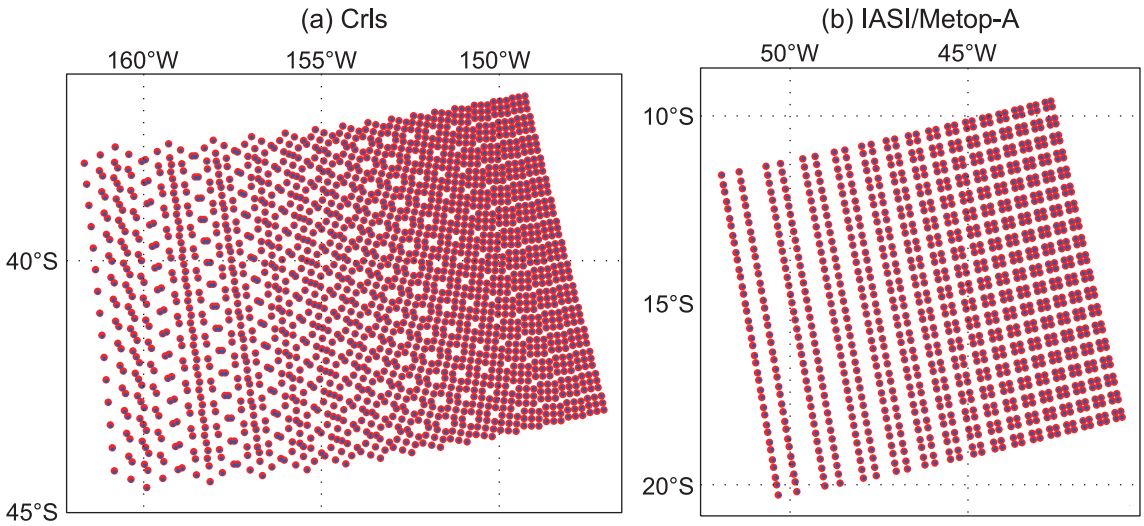

Fig. 3. Validation of simulated (a) CrIS and (b) IASI/MetOp-A orbits using observations. The red dots represent the simulated locations of CrIS and IASI/MetOp-A FOVs, and blue dots represent observations. The CrIS time is 2354:10 UTC 23 September 2014, and the IASI/MetOp-A time is 0023:58 UTC 24 September 2014. Only half of the scan lines are shown due to symmetry.

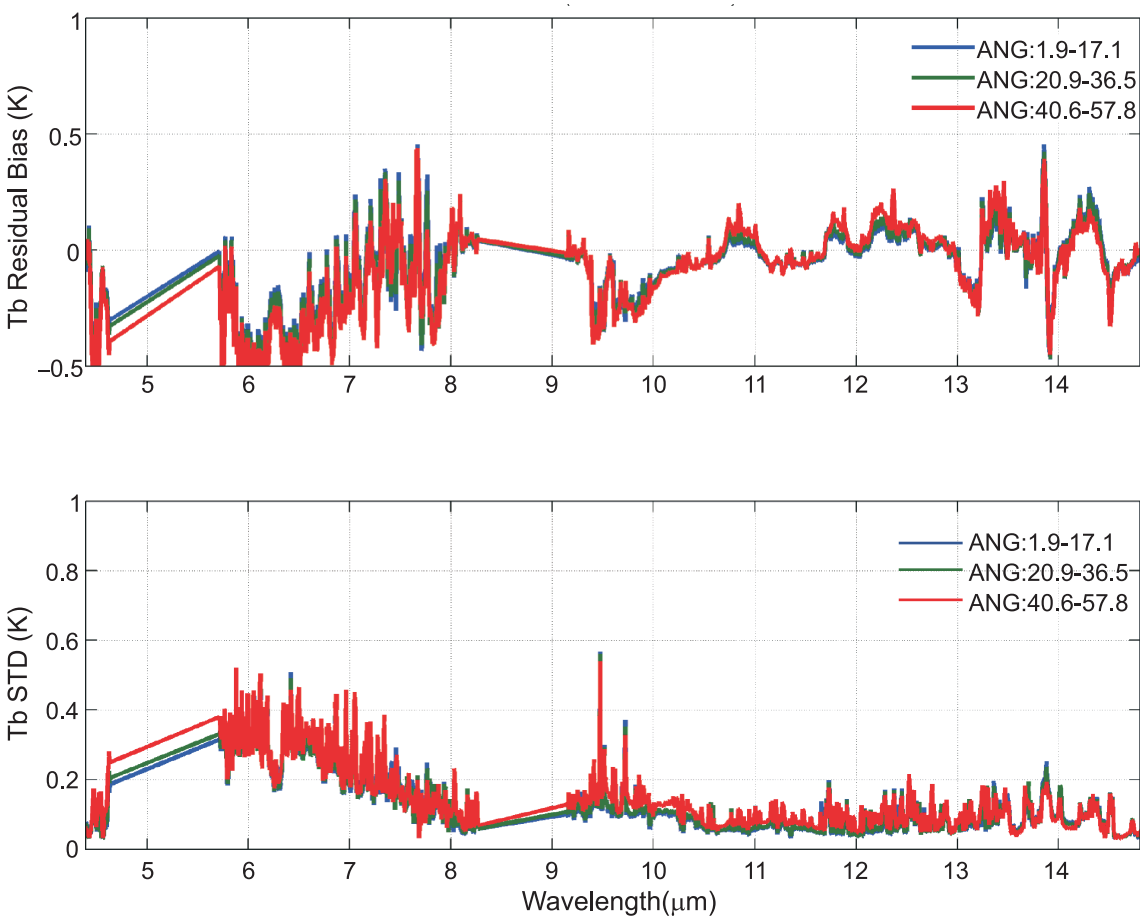

Fig. 4. Clear-sky RTM comparison (bias in upper panel; STD in lower panel) between SARTA and CRTM with different satellite viewing angle zones (1.9°–17.1°, 20.9°–36.5° and 40.6°–57.8°) for CrIS. The UW SeeBor database containing 15 704 global profiles are used in the simulation.

gion, without any obvious angle dependency. The bias shows some spectral variations, especially in the longwave CO_2 region (> 13 μm). However, most of the bias is within ±0.3 K. The water vapor channels have a slightly larger bias, but in general are within ±0.5 K. The standard deviation (STD) shows very good agreement between SARTA and CRTM. There is no strong spectral dependency shown, except on some of the absorption lines (water vapor, ozone and CO_2). These small but substantial differences between SARTA and CRTM are important for OSSE studies. In an OSSE, it is generally preferred that the same RTM is not used in the radiance simulation and assimilation—the equivalent of assuming a perfect RTM, which is not true in reality. The HIRTM requires four parameters of clouds in order to perform the cloudy radiative transfer calculation: the effective cloud particle diameter; cloud optical thickness; effective cloud-top pressure; and cloud phase (Wei et al., 2004). All four parameters can be calculated from the hydrometer profiles in the NR (Li et al., 2017). In addition to using the HIRTM for AIRS, CrIS and two IASIs, CRTM V2.1.3, with optical depth in absorber space (ODAS) coefficients, are used to simulate the radiances for ATMS and six AMSU-As from MetOp-A/B and the NOAA satellites. In total, 11 existing LEO instruments are simulated to represent the existing LEO capability (Table 1).

2.4. *Synthetic observation simulation*

Key parameters from the NR used for the synthetic radiance simulation are listed in Table 2. Additional ancillary data include the climatological ozone profile and the UW High Spectral Resolution IR emissivity database. All profiles are linearly interpolated from 51 WRF model levels to 101 RTM levels. Levels above the model top are filled with climatological temperature and water vapor profiles. An overall shift of the climatological profiles is performed to ensure

Table 1. Simulated LEO satellite radiances assimilated in the experiments.

Instrument	Host satellite
AMSU-A	NOAA-15, NOAA-18, NOAA-19, MetOp-A, MetOp-B, Aqua
IASI	MetOp-A, MetOp-B
AIRS	Aqua
ATMS	Suomi-NPP
CrIS	Suomi-NPP

Table 2. Key parameters from the WRF-NMM forecast used in the radiative transfer calculation.

Clear parameters	Cloud parameters
Surface skin temperature (K)	Cloud water mixing ratio (kg kg^{-1})
Temperature profile (K)	Rain water mixing ratio (kg kg^{-1})
Water vapor mixing ratio profile (kg kg^{-1})	Ice mixing ratio (kg kg^{-1})
Surface pressure (Pa)	Graupel mixing ratio (kg kg^{-1})
	Snow mixing ratio (kg kg^{-1})

smooth change around the model top. Use of climatological profiles in those upper levels has very minor impacts on the radiative transfer calculations.

Once the NR and orbits are ready, the synthetic radiance can be simulated via the following steps. For a given geolocation, the FOV size is calculated based on the viewing angle and the provided nadir FOV size (the spatial resolution). With the FOV size known, all NR pixels falling into that FOV will be used to calculate the mean thermodynamic and hydrometer profiles as well as surface parameters, which are used as inputs for the RTM. Random noise is added based on the instrument specification of the Noise Equivalent delta Radiance for IR or Noise Equivalent delta Temperature for microwave. All LEO radiances are converted to Binary Universal Form for the Representation of meteorological data (BUFR) format.

Simulating a future GEO hyperspectral IR sounder follows a more straightforward two-step process. In the first step, the radiance simulation is performed for every grid point in the NR. The satellite and solar geometries for each grid point can be calculated with the known satellite longitude and observation time. In the second step, a linear spatial interpolation is used to convert the simulated radiances to satellite observation locations. This step actually decreases the spatial resolution from the NR to the satellite sensor. All hyperspectral IR sounder radiances, from both GEO and LEO, are simulated using the HIRTM. All others are simulated using CRTM ODAS coefficients.

For synthetic Global Telecommunication System (GTS) observations, only the RAOB profiles of temperature, moisture, and U/V (zonal/meridional) winds are simulated using the nearest profile from the NR at real RAOB locations extracted from real GTS data with random Gaussian noise added. The T/Q (temperature/moisture) random noise is generated using eigenvectors derived from the UW-Madison SeeBor database (Seemann et al., 2008). A similar technique has been used before to generate simulated GFS forecast profiles from RAOB profiles (Jin et al., 2008; Li et al., 2009). The overall STDs of error for temperature and moisture profiles are 1 K and 10% in relative humidity—the same as those used in the Community Gridpoint Statistical Interpolation (GSI) for PrepBUFR data (Keyser, 2018). The dry bias is not considered in the moisture simulation. Random noise for wind is added in a similar way, but with eigenvectors derived from the GFS forecast. The advantage of eigenvectors instead of random noise at each level is that the former includes vertical correlation, which is more realistic than the latter. The synthetic RAOB data are generated every 6 h, with the majority of the data from 0000 and 1200 UTC.

2.5. *Verification of simulated radiances*

Validating the simulated synthetic radiances follows two steps: validating the RTM and validating the simulated radiances. The first step ensures the radiance simulation is carried out properly by the RTM, in both clear and cloudy skies. Usually, the validation is performed by comparing with real observations or simulations from other RTMs, like the line-by-line RTM. Both the CRTM (Chen et al., 2010, 2012) and the HIRTM (Li et al., 2017) have been validated before. The second step ensures the simulated radiances are reasonable. This means that both the NR and the RTM have to be reasonable.

In this study, the future GEO hyperspectral IR sounder is assumed to be IASI at the GOES-16 on-orbit check-out location at 89.5°W, with a spatial resolution of 4 km and temporal resolution of 1 h. The validation of the simulated synthetic radiances is difficult because the NR has nothing to do with reality; there are no real observations that are close to the HRNR that can be used for direct validation. Besides, there are no geostationary satellite radiance observations from 89.5°W at the HRNR time. However, one can still use real observations to indirectly verify the simulated GEO IASI radiances.

To demonstrate that, another set of GEO IASI radiances are simulated by placing IASI at the location of GOES-12 (75°W). The synthetic GEO IASI radiances, which are simulated from the HRNR using the HIRTM, are further convolved with the GOES-12 Imager SRF to generate the simulated GOES-12 Imager radiances. Instead of a direct comparison between the simulation and the observation (the two are totally different), the focus is on whether the temporal variation of the simulated radiances is similar to reality. If the temporal variation of the HRNR is not realistic, or if the simulated radiances are not realistic, it is unlikely the temporal variation of the simulated radiances will be in a pattern similar to the real observations. Figure 5 shows that the temporal variations of the simulations for GOES-12 Imager "water vapor" band 3 (6.48 μm) and the "longwave window" band 4 (10.71 μm) are highly similar to those of the observations. The temporal variation is defined as $\mathrm{Tb}_{t2} - \mathrm{Tb}_{t1}$, where t2 − t1 is 60 minutes for the GOES-12 Imager. Comparisons of band 3 (6.48 μm) and band 6 (13.31 μm), and band 4 (10.71 μm) and band 6 (13.31 μm), also show similar agreement. The similarity of the temporal variations between the simulation and the observation indicates that: (1) the two simulated GOES-12 Imager channels are consistent with each other (both are reasonably simulated); (2) the simulated radiances capture the real temporal variation reasonably well; and (3) the temporal variation of the thermodynamic information from the HRNR is realistic. With this agreement between the simulation and observation for the GOES-12 Imager, it is reasonable to believe the GEO IASI synthetic radiances from 89.5°W are reasonably simulated.

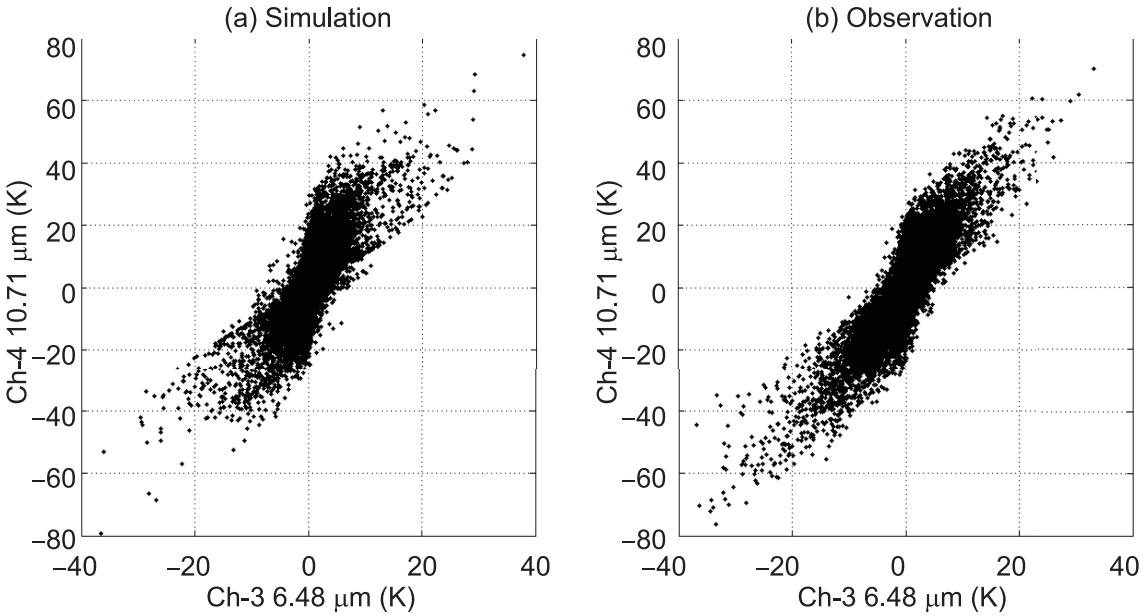

Fig. 5. Temporal variation of GOES-12 Imager bands 3 and 4 from the (a) simulation and (b) observations. The similarity between the simulation and observation indicates channels 3 and 4 are reasonably simulated from the NR.

2.6. *Synthetic sounding retrievals*

Similar to Jones et al. (2017), synthetic atmospheric sounding retrievals are generated using a simple linear regression technique in clear sky. While assimilating radiances and assimilating sounding retrievals for the hyperspectral IR sounders are theoretically equivalent (Migliorini, 2012), the latter does have some advantages at the current stage. For example, in the retrieval, more channels could be used, while the radiance assimilation is limited by channel correlation and computational resources. In particular, for future GEO hyperspectral IR sounders, which have finer spatial resolution and higher temporal resolution, there will be significantly more observations than for existing LEO sounders. The retrieval greatly reduces the computational burden, whilst at the same time retaining most of the information. The retrieved atmospheric temperature and moisture soundings, together with the simulated RAOBs, are converted to PrepBUFR.

3. Assimilation experiments and impact study

For assessing the impact on LSS forecasts, all simulated synthetic observations are converted to either BUFR or PrepBUFR. The BUFR data include simulated LEO radiances from IASI on MetOp-A/B, CrIS, AIRS, ATMS, and AMSU-A on the MetOp-A/B and NOAA satellites (Table 1). The PrepBUFR data include GEO IASI sounding retrievals and RAOBs. While a calibration is preferred for a rigorous OSSE, it is noted that the rOSSE system used in this study is not calibrated. The calibration requires carefully tuning the simulated observation errors so that they have similar impact as in the real world. The short lifetime of the HRNR (less than three days) makes it difficult to perform a statistically sound calibration. For that reason, many rOSSE studies do not perform a calibration (Cintineo et al., 2016; Jones et al., 2017; Zhang et al., 2017), especially when the two respective models for the NR and forecast impact are different.

3.1. *Experimental design*

The GSI three-dimensional variational system, V3.3, is used as the data assimilation model, which is supported by the Development Testbed Center for community research and study based on the NOAA operational data assimilation system. It can assimilate various kinds of observations, including conventional data, satellite radiances, radar reflectivity, etc. The GEO IASI soundings are assimilated as radiosonde profiles in this study in the GSI model. Considering this study focuses on severe weather forecasting in a regional model, the background error covariance from the North American Mesoscale Forecast System (NAM) is adopted in the experiments. The enhanced bias correction scheme (Zhu et al., 2014) is applied for the assimilation of satellite radiances, and the bias coefficients are updated for every cycling run. The same bias correction scheme is used for all experiments.

To avoid the identical twin problem in OSSEs, the Advanced Research version of the WRF model (WRF-ARW), V3.6.1, is chosen as the regional NWP forecast model for the LSS simulation. The global OSSE analysis data are used to initialize the forecast domain and provide the boundary conditions for the rOSSE. No synthetic observations from the global OSSE are used in this study. Compared with WRF-NMM, used for NR generation, the WRF-ARW has a coarser horizontal spatial resolution (9 km), smaller coverage (450×280 grid points) (Fig. 1), and different schemes are used, including the New Thompson scheme for microphysics, Rapid Radiative Transfer Model-Global (RRTMG) for the longwave radiation scheme, RRTMG for the shortwave radiation scheme, the Yonsei University scheme for the

planetary boundary layer, and the Kain–Fritsch scheme for cumulus parameterization.

Figure 6 is a flow chart of the experiments for LSS simulation. The model starts at 0600 UTC 26 May, with a 6-h spin-up, and the cycled data assimilation is performed from 1200 UTC 26 May to 0000 UTC 27 May, followed by an 18-h forecast to 1800 UTC 27 May. The 6-h cycling is chosen to be consistent with the NAM and GFS. For the control (CNTRL) experiments, the data assimilated include simulated radiosonde observations (temperature, moisture, and U/V winds) and simulated satellite radiance observations from the sensors listed in Table 1. This represents the existing capability. The experiment with GEO IASI soundings (GEO, for short), as additional observations, represents the capability from one future geostationary hyperspectral IR sounder. The temperature and moisture soundings from GEO IASI are assimilated only from the surface to 200 hPa, with a relaxed observational error covariance [four times the original root-mean-square difference (RMSD) calculated from comparison with the NR]. Due to the high density of the GEO IASI data (4-km spatial resolution), the profiles are thinned every 60 km at first. Impacts from different combinations of the assimilation cycle frequency and thinning distance are further discussed in a later section.

3.2. *Impact on LSS forecasts*

The focus of this study is to show the impact of a GEO hyperspectral IR sounder over existing LEO sounders for LSS forecasts. Compared with LEO, GEO increases the spatial coverage for the regional model. Despite the global coverage from LEO, GEO is capable of providing more frequent full-disk coverage for an LSS study. Figure 7 shows the data coverage of GEO IASI temperature at 500 hPa at 1200 UTC 26 May (with a 60-km thinning). The GEO IASI data are available for the whole model domain, and only data under clear skies are assimilated in the GSI model. The assimilated GEO IASI soundings directly affect thermodynamic and dynamic fields at the analysis time, although the percentage of data assimilated is only 0.125% (see Table 3). The temperature field and the differences between the HRNR and experiments at 1200 UTC 26 May are shown in Fig. 8. Compared with the HRNR, the temperature fields of the CNTRL are warmer in the western part of the model domain. The temperature RMSD is 0.55 K, and the STD is 0.54 K. With the assimilation of the GEO IASI soundings, the warm bias at the

Table 3. Reduction of the final normalized RMSD in percentage terms (%, first number) by different experiments (thinning distance and refresh rate) compared to the CNTRL run, and the percentage (%, second number) of the assimilated observations compared with all available clear-sky GEO IASI soundings within the model domain for all cycle steps.

	15 km		30 km		60 km		120 km	
	RMSD	Obs %	RMSD	Obs %	RMSD	Obs %	RMSD	Obs %
3 h	3.87	1.348	4.60	0.406	4.22	0.124	3.44	0.038
6 h	4.41	1.348	3.83	0.407	3.56	0.125	3.20	0.038

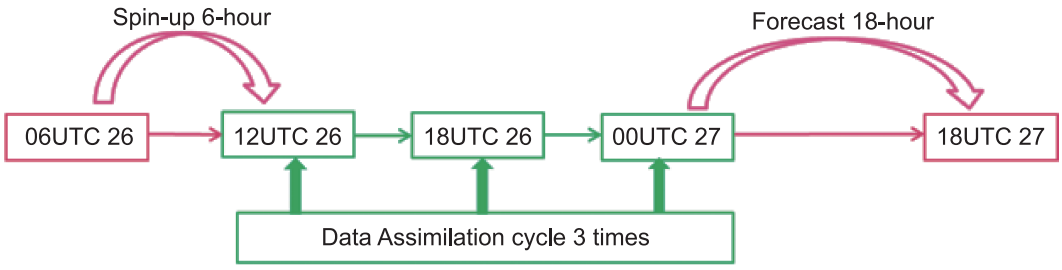

Fig. 6. Flow chart of the experimental design.

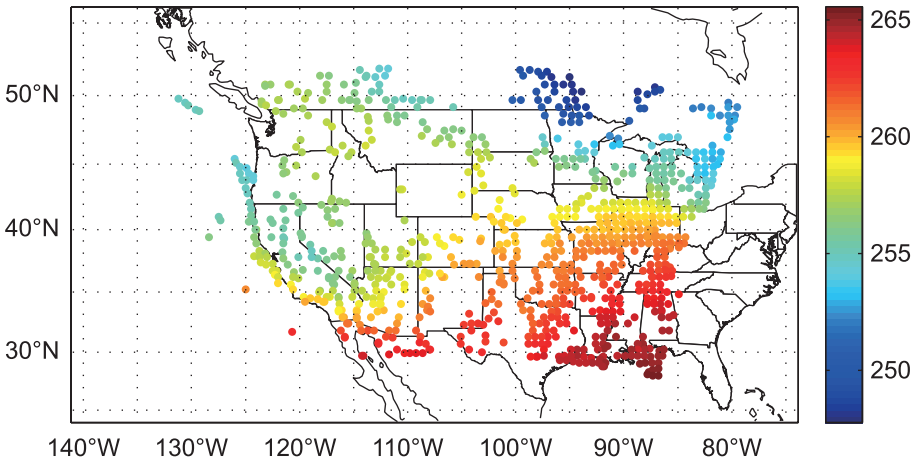

Fig. 7. Data coverage of the retrieval temperature (units: K) at 500 hPa at 1200 UTC 26 May.

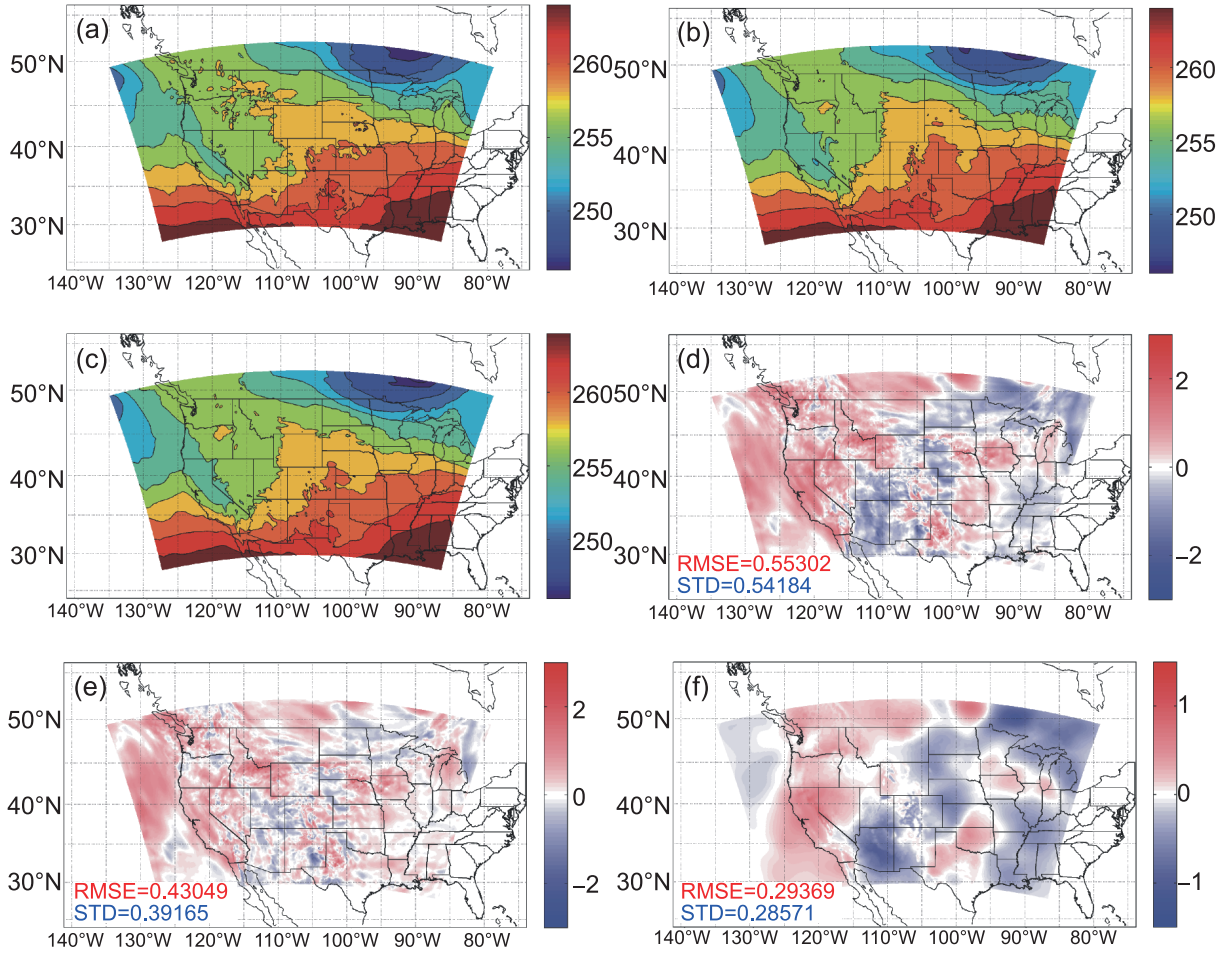

Fig. 8. Temperature at 500 hPa of (a) NR, (b) CNTRL and (c) GEO IASI at 1200 UTC 26 May, and the differences between the NR and experiments for temperature at 500 hPa: (d) NR−CNTRL; (e) NR−GEO; (f) GEO−CNTRL (units: K).

western end of the model domain is smaller, and the temperature RMSD is reduced to 0.43 K, and the STD to 0.39 K. The RMSD is reduced by 22.16%, and the STD reduced by 27.72%. A similar reduction in RMSD can be seen at the two other assimilation times.

To further assess the impact of GEO IASI soundings on the analyzed temperature field, the temperature RMSD profile between the HRNR and experiments is calculated from 200 hPa to 1000 hPa at 1200 and 1800 UTC 26 May, and 0000 UTC 27 May (Fig. 9). The blue dashed line represents CNTRL and the red line GEO IASI. The temperature fields in the whole model domain are used for verification of the analysis fields. At all three analysis times, GEO has a smaller RMSD than CNTRL for the whole vertical profile from 200 to 1000 hPa. The largest RMSD differences are always found at around 200 hPa, which indicates the temperature adjustments with assimilating GEO IR soundings are larger near the top of the troposphere than at lower levels. For the RMSD of GEO IASI, an average reduction of 0.15 K throughout the profiles is found over CNTRL. Based on the comparison with the HRNR, assimilating GEO IASI soundings brings the temperature fields in the troposphere closer to the HRNR, and reduces the difference between CNTRL and the HRNR.

Instead of showing further results from individual parameters, an overall evaluation strategy is carried out. The purpose is to use one single parameter to characterize the overall impact for the LSS simulations in the whole domain, which includes most of the important analysis/forecast parameters. For that purpose, the following parameters are selected: the temperature, relative humidity, and U/V winds at four standard atmospheric levels (250 hPa, 500 hPa, 700 hPa and 850 hPa) to represent the atmospheric thermodynamic fields of the whole domain. In addition, convective available potential energy (CAPE), convective inhibition (CIN), and helicity are used to reflect the environmental instabilities, which are often used by forecasters to make predictions, as well as precipitation, which is an important forecast parameter for LSSs.

The RMSDs are calculated for each parameter for the whole model domain using the HRNR as a reference, except for precipitation; the results are shown in Table 4. Due to the high temporal and spatial variability of precipitation, the equitable threat score (ETS) is often used to characterize both the precipitation amount and pattern (Hamill, 1999). To be consistent with the RMSD for which lower values indicate better results, 1-ETS, which is the difference between one and ETS scores of 0.1 mm as the threshold, is used. Notice the

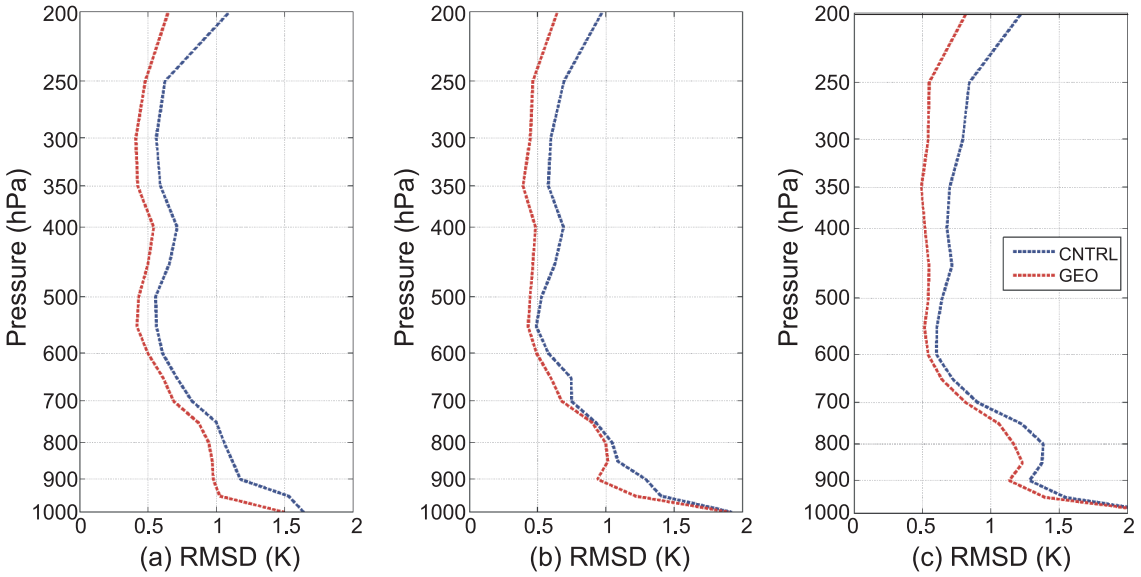

Fig. 9. Temperature RMSD between NR and CNTRL (blue), and between NR and GEO (red) from 200 hPa to 1000 hPa at (a) 1200 UTC 26 May 26, (b) 1800 UTC 26 May, and (c) 0000 UTC 27 May.

Table 4. RMSD of the parameters between the NR and experiments. Bold values are the smaller ones between the two experiments. Bold values for percentage change indicate improvement by GEO.

Variables	CNTRL	GEO	Percentage change
Temperature (K)	0.8544	**0.7933**	**7.15%**
Relative Humidity (%)	13.1601	**12.5208**	**4.86%**
U-wind (m s^{-1})	2.6645	**2.5073**	**5.9%**
V-wind (m s^{-1})	2.7777	**2.5832**	**7%**
CAPE (J kg^{-1})	**19.7638**	19.9281	−0.83%
CIN (J kg^{-1})	18.1798	**17.8915**	**1.59%**
Helicity (m^2 s^{-2})	32.9175	**32.5925**	**0.99%**
Precipitation 1-ETS	0.6326	**0.6252**	**1.17%**

temperature, relative humidity and winds are the mean value of the four standard levels. In Table 4, the smaller values between the two experiments are in bold, and the percentage changes are also listed in the last column. For all parameters except CAPE, GEO IASI shows better results than CNTRL. For example, for temperature, assimilating GEO IASI soundings reduces the RMSD by 7.15%, relative humidity by 4.86%, U-wind by 5.9%, V-wind by 7%, CIN by 1.59%, etc. However, it is still impossible to combine different parameters together due to the different units for the parameters. Therefore, a normalization process is carried out to ensure the sum of the square equals 1 for each parameter, including 1-ETS. And the final nominalized RMSD is calculated using a weighted average:

- Thermodynamic parameters ($T/Q/U/V$), 50%
- CAPE, 10%
- CIN, 10%
- Helicity, 10%
- Precipitation 1-ETS, 20%

The selected instabilities (10%) and precipitation 1-ETS (20%) are given relatively large weights because of their importance in LSS simulation, especially the precipitation. $T/Q/U/V$ are averaged together with a 50% weight. The calculation is performed at the last analysis time (0000 UTC 27 May) and every 6-h forecast (0600, 1200, and 1800 UTC 27 May). The precipitation ETSs are calculated for every 6-h accumulated rainfall at 0600, 1200 and 1800 UTC 27 May.

Using the above method, the final normalized RMSD of CNTRL and GEO IASI are calculated. Assimilating GEO IASI soundings is effective in reducing the normalized RMSD from 0.72 to 0.69, which reduces the total normalized RMSD by around 3.56%. The reduction is mainly from the thermodynamic information, which indicates assimilating GEO IASI soundings may benefit the temperature, relative humidity and winds substantially. Overall, the GEO IASI soundings are adding value to the LSS simulation for both the analysis and forecast compared with CNTRL.

4. Analysis and discussion

Despite a spatial resolution of 4 km and temporal resolution of 1 h, the GEO IASI soundings are assimilated with a thinning of 60 km and a 6-h cycling. This means that about 0.1% of the clear-sky observations are assimilated; the majority of the observations are not used. This is not the best way to take advantage of the high temporal and spatial resolutions from GEO. Thinning and relatively large cycling hours can help reduce the impacts from the error correlation (Liu and Rabier, 2002, 2003) in observations, the gravity wave, and initial imbalances in the model (Lynch and Huang, 1992; Benjamin et al., 2004). However, it is important to explore how current assimilation systems and forecast models can take advantage of the high temporal and spatial resolutions from a future GEO hyperspectral IR sounder.

To study the impact of different thinning distances and cy-

cling hours, more experiments are carried out with different thinning distances: 15, 30, 60, and 120 km. For each experiment, the cycling hours of both 3 and 6 h are tested. In total, there are eight experiments in addition to the CNTRL run. Table 3 shows the percentage of observations assimilated, as compared with all available clear-sky GEO IASI soundings within the model domain for all cycled steps. With the same thinning distance, the cycling hour has little impact on the percentage of observations assimilated. However, for a fixed cycling hour, the thinning distance has significant impacts; as the thinning distance halves, the percentage of assimilated observations increases at a rate slightly less than four due to clouds. To quantify the impact of the increased assimilated observations, a final normalized RMSD (not shown) is calculated for each experiment and the CNTRL. The reductions of RMSD in percentage terms for all experiments, compared with the CNTRL, are shown in Table 3. Overall, all experiments show a positive impact from assimilating GEO IASI soundings (the final normalized RMSD is always smaller than the CNTRL), regardless of the thinning distance and cycling hours. When the assimilation cycle is every 6 h, a smaller thinning distance leads to better analysis/forecast results. This is reasonable because there is no error correlation added in the simulated radiance observations. Some error correlations might exist in the GEO IASI sounding retrievals from the retrieval algorithm. However, with a cycle of 6 h, WRF-ARW is able to manage it. When the assimilation cycle is every 3 h, a smaller thinning distance appears to help from 120 km down to 30 km. With a thinning distance of 30 km, the GEO IASI soundings have the largest impact of 4.60% over the CNTRL. This means a reduction in the normalized RMSD of the analysis and forecast by 4.60% from the GEO IASI soundings. Compared with a cycle of 6 h and a thinning of 60 km, there is a slightly more than 1% RMSD reduction. A further smaller thinning distance appears to reduce the positive impact from GEO IASI soundings. A couple of possible reasons may explain this result. One is probably due to the gravity wave and spatial error correlations, which become more difficult for WRF-ARW to handle within 3 h. To further shorten the cycling hour and the thinning distance may require some numerical techniques, such as a digital filter (Huang et al., 2007; Peckham et al., 2016), to remove the exhibited noise from the imbalance in the model forecasts, which is beyond the scope of this study and therefore not discussed any further. Another is the WRF-ARW model resolution (9 km) used in the study. Thinning GEO IASI at 15 km is very close to the model resolution. Combining these dense observations with the high frequency cycle assimilation (here, 3 h) could make the model dynamical adjustment difficult from the data influence. There should be an optimal balance among the data density, data assimilation cycle and model resolution. In our cases, 30-km thinning with 3-h cycling assimilation is the best, and 15-km thinning with 6-h cycling assimilation is the second best. In general, with an appropriate model resolution, the higher spatial resolution GEO IASI soundings and the higher assimilation cycle may increase the forecast skill.

OSSEs can provide quantitative information on observing system impacts for new as well as current observing systems. It can also be used for data assimilation system diagnosis and methodology improvement. Information from OSSEs can lead to better planning and decisions. Quick rOSSEs have the advantage of being cheap and fast to perform, and can sometimes be used to answer questions relating to a particular storm or to demonstrate potential. However, quick rOSSEs are limited in utility since they typically cannot be used to establish statistically significant quantitative results. Both global full OSSEs and quick rOSSEs are helpful for planning and decision making, while the planning and decision making cannot fully rely on OSSE results for three reasons. First, OSSEs have limitations: an NR might not necessarily reflect nature in reality, especially for mesoscale and small-scale weather systems. For example, an NR might have difficulty in simulating the storm intensity due to a limitation of the NWP model used to create the NRs. In addition, the current assimilation system used for impact studies might not be advanced enough to account for the full benefits of future advanced observing systems. Third, OSSEs mainly target NWP applications, while observations from an instrument may have much wider applications. For example, high-density observations can be used to provide warning information in the pre-convection environment (Ferretti and Faccani, 2005, Li et al., 2011), and can also be used for environment and climate monitoring.

5. Summary and future work

A quick rOSSE framework has been developed, including NR generation, orbit simulator, synthetic observation simulation and validation, and impact study. The application to a case study of an LSS using GEO IASI observations has been carried out. GEO IASI has larger spatial coverage and higher temporal resolution, compared with LEO advanced IR sounders, for regional NWP models. The impact study shows that GEO IASI may add substantial positive value to the analysis and forecasting of the thermodynamic parameters of $T/Q/U/V$. The evaluation based on the combined normalized RMSD from different parameters indicates an overall positive impact on the LSS analysis and forecast for the case demonstrated. The reduction in the normalized RMSD in the analysis and forecast is 3.56%. In addition, experiments with different thinning distances and assimilation cycling hours reveal that more frequent assimilation and a shorter thinning distance may further increase the positive impact from GEO IASI with the current GSI/WRF-ARW system. However, denser and more frequent assimilated observations also poses a significant burden on the assimilation and forecast systems, especially in handling the spatial error correlation in observations and gravity waves with a static background error covariance matrix, which could hinder the positive impact from GEO IASI. The peak reduction of 4.60% in the normalized RMSD is found with a thinning distance of 30 km and a cycle of 3 h. Any further reduction in thinning distance and cycling hour should also consider the model resolution used.

It should be noted that this is a single case study; the results do not provide statistical significance. Ideally, more cases should be used, but identifying typical LSS cases from a global NR is not easy due to the fact that global NRs are limited in simulating strong LSSs. Nevertheless, the case study demonstrates the potential value-added impact from GEO hyperspectral IR sounder data on LSSs.

To improve background error representativeness, future work should use a hybrid/ensemble data assimilation system with a flow-dependent background error covariance. Improving sounding retrievals using the one-dimensional variational method (Li et al., 2000), expanding soundings into cloudy skies (Li et al., 2009, 2016; Wang et al., 2014, 2015, 2017), and including geostationary imager radiances (Honda et al., 2018a, 2018b) for assimilation will also be conducted. Comparison between direct sounding radiance assimilation and retrieval assimilation should also be included, with an appropriate experimental design. Another important future aim is to assimilate atmospheric motion vectors (AMVs) derived from water vapor soundings; the AMVs from continuous water vapor measurements are an important feature of GEO advanced IR sounders, which could further benefit LSS forecasts.

Acknowledgements. This work is partly supported by the NESDIS OPPA OSSE program (Grant No. NA15NES4320001). The views, opinions, and findings contained in this report are those of the authors and should not be construed as an official NOAA or U. S. government position, policy, or decision. Thanks to the Joint Center for Satellite Data Assimilation for providing the "S4" supercomputer [Supercomputer for Satellite Simulations and Data Assimilation Boukabara et al. (2016b)], physically located at SSEC, University of Wisconsin-Madison, as the main computational resource for this research study.

REFERENCES

Atlas, R., 1997: Atmospheric observations and experiments to assess their usefulness in data assimilation (gtSpecial Issuelt-Data assimilation in meteology and oceanography: Theory and practice). *J. Meteor. Soc. Japan*, **75**, 111–130, https://doi.org/10.2151/jmsj1965.75.1B_111.

Atlas, R., L. Bucci, B. Annane, R. Hoffman, and S. Murillo, 2015: Observing system simulation experiments to assess the potential impact of new observing systems on hurricane forecasting. *Marine Technology Society Journal*, **49**, 140–148.

Auligné, T., F. Rabier, L. Lavanant, and M. Dahoui, 2003: First results of the assimilation of AIRS data in Météo-France Numerical Weather Prediction model. *Proc. 13th International TOVS Study Conf.*, Adele, Canada.

Benjamin, S. G., and Coauthors, 2004: An hourly assimilation–forecast cycle: The RUC. *Mon. Wea. Rev.*, **132**, 495–518, https://doi.org/10.1175/1520-0493(2004)132<0495:AHACTR>2.0.CO;2.

Bessho, K., and Coauthors, 2016: An introduction to himawari-8/9 - Japan's New-Generation Geostationary Meteorological Satellites. *J. Meteor. Soc. Japan*, **94**, 151–183.

Boukabara, S., and Coauthors, 2016a: Community global observing system simulation experiment (OSSE) package (CGOP): Description and usage. *J. Atmos. Oceanic Technol.*, **33**, 1759–1777, https://doi.org/10.1175/JTECH-D-16-0012.1.

Boukabara, S., and Coauthors, 2016b: S4: An O2R/R2O infrastructure for optimizing satellite data utilization in NOAA numerical modeling systems: A step toward bridging the gap between research and operations. *Bull. Amer. Meteor. Soc.*, **97**, 2359–2378, https://doi.org/10.1175/BAMS-D-14-00188.1.

Boukabara, S., and Coauthors, 2018: Community global observing system simulation experiment (OSSE) package CGOP: Perfect observations simulation validation. *J. Atmos. Oceanic Technol.*, **35**, 207–226, https://doi.org/10.1175/JTECH-D-17-0077.1.

Cardinali, C., 2009: Monitoring the observation impact on the short - range forecast. *Quart. J. Roy. Meteor. Soc.*, **135**, 239–250, https://doi.org/10.1002/qj.366.

Chahine, M. T., and Coauthors, 2006: AIRS: Improving weather forecasting and providing new data on greenhouse gases. *Bull. Amer. Meteor. Soc.*, **87**, 911–926, https://doi.org/10.1175/BAMS-87-7-911.

Chen, Y., Y. Han, P. Van Delst, and F. Z. Weng, 2010: On water vapor Jacobian in fast radiative transfer model. *J. Geophys. Res.*, **115**, https://doi.org/10.1029/2009JD013379.

Chen, Y., Y. Han, and F. Z. Weng, 2012: Comparison of two transmittance algorithms in the community radiative transfer model: Application to AVHRR. *J. Geophys. Res.*, **117**, https://doi.org/10.1029/2011JD016656.

Cintineo, R. M., J. A. Otkin, T. A. Jones, S. Koch, and D. J. Stensrud, 2016: Assimilation of synthetic GOES-R ABI infrared brightness temperatures and WSR-88D radar observations in a high-resolution OSSE. *Mon. Wea. Rev.*, **144**(9), 3159–3180, https://doi.org/10.1175/MWR-D-15-0366.1.

Collard, A. D., and A. P. McNally, 2009: The assimilation of infrared atmospheric sounding interferometer radiances at ECMWF. *Quart. J. Roy. Meteor. Soc.*, **135**, 1044–1058, https://doi.org/10.1002/qj.410.

Ferretti, R., and C. Faccani, 2005: Data assimilation of high-density observations. II: Impact on the forecast of the precipitation for the MAP/SOP IOP2b. *Quart. J. Roy. Meteor. Soc.*, **131**, 43–61, https://doi.org/10.1256/qj.03.56B.

Gambacorta, A., and Coauthors, 2014: An experiment using high spectral resolution CrIS measurements for atmospheric trace gases: Carbon monoxide retrieval impact study. *IEEE Geoscience and Remote Sensing Letters*, **11**, 1639–1643, https://doi.org/10.1109/LGRS.2014.2303641.

Gelaro, R., and Coauthors, 2015: Evaluation of the 7-km GEOS-5 nature run. NASA/TM-2014-104606/VOL36, NASA Goddard Space Flight Center, 285 pp.

Hamill, T. M., 1999: Hypothesis tests for evaluating numerical precipitation forecasts. *Wea. Forecasting*, **14**(2), 155–167, https://doi.org/10.1175/1520-0434(1999)014<0155:HTFENP>2.0.CO;2.

Hannon, S. E., L. L. Strow, and W. W. McMillan, 1996: Atmospheric infrared fast transmittance models: A comparison of two approaches. *Proc. SPIE Volume 2830, Optical Spectroscopic Techniques and Instrumentation for Atmospheric and Space Research II*, Denver, CO, United States, SPIE, 94–105, https://doi.org/10.1117/12.256106.

Hilton, F., N. C. Atkinson, S. J. English, and J. R. Eyre, 2009: Assimilation of IASI at the Met Office and assessment of its impact through observing system experiments. *Quart. J. Roy. Meteor. Soc.*, **135**, 495–505, https://doi.org/10.1002/qj.379.

Hilton, F., and Coauthors, 2012: Hyperspectral Earth observation from IASI: Five years of accomplishments. *Bull. Amer. Me-*

teor. Soc., **93**, 347–370, https://doi.org/10.1175/BAMS-D-11-00027.1.

Hoffman, R. N., and R. Atlas, 2016: Future observing system simulation experiments. *Bull. Amer. Meteor. Soc.*, **97**, 1601–1616, https://doi.org/10.1175/BAMS-D-15-00200.1.

Honda, T., and Coauthors, 2018a: Assimilating all-sky *Himawari*-8 satellite infrared radiances: A case of typhoon Soudelor (2015). *Mon. Wea. Rev.*, **146**, 213–229, https://doi.org/10.1175/MWR-D-16-0357.1.

Honda, T., S. Kotsuki, G. Y. Lien, Y. Maejima, K. Okamoto, and T. Miyoshi, 2018b: Assimilation of Himawari-8 all-sky radiances every 10 minutes: Impact on precipitation and flood risk prediction. *J. Geophys. Res.*, **123**, 965–976, https://doi.org/10.1002/2017JD027096.

Huang, X. Y., M. Chen, W. Wang, J.-W. Kim, B. Skamarock, and T. Henderson, 2007: Development of Digital Filter Initialization for WRF and its implementation at IUM. *Preprints: 8th Annual WRF User's Workshop*, NCAR, Boulder, CO, NCAR.

Jin, X., J. Li, T. J. Schmit, J. L. Li, M. D. Goldberg, and J. J. Gurka, 2008: Retrieving clear-sky atmospheric parameters from SEVIRI and ABI infrared radiances. *J. Geophys. Res.*, **113**, D15310, https://doi.org/10.1029/2008JD010040.

Jones, T. A., S. Koch, and Z. L. Li, 2017: Assimilating synthetic hyperspectral sounder temperature and humidity retrievals to improve severe weather forecasts. *Atmospheric Research*, **186**, 9–25, https://doi.org/10.1016/j.atmosres.2016.11.004.

Joo, S., J. Eyre, and R. Marriott, 2013: The impact of Metop and other satellite data within the Met Office global NWP system using an Adjoint-based sensitivity method. *Mon. Wea. Rev.*, **141**, 3331–3342, https://doi.org/10.1175/MWR-D-12-00232.1.

Keyser, D., 2018: PREPBUFR processing at NCEP. Tech. rep., National Centers for Environmental Prediction. Available online at http://www.emc.ncep.noaa.gov/mmb/data_processing/prepbufr.doc/document.htm.

Le Marshall, J., and Coauthors, 2005: Impact of atmospheric infrared sounder observations on weather forecasts. *Eos*, **86**(11), 109–116, https://doi.org/10.1029/2005EO110002.

Le Marshall, J., and Coauthors, 2006a: Improving global analysis and forecasting with AIRS. *Bull. Amer. Meteor. Soc.*, **87**, 891–895, https://doi.org/10.1175/BAMS-87-7-891.

Le Marshall, J., J. Jung, T. Zapotocny, J. Derber, R. Treadon, S. Lord, M. Goldberg, and W. Wolf, 2006b: The application of AIRS radiances in numerical weather prediction. *Aust. Meteor. Mag.*, **55**, 213–217.

Li, J., W. W. Wolf, W. P. Menzel, W. J. Zhang, H.-L. Huang, and T. H. Achtor, 2000: Global soundings of the atmosphere from ATOVS measurements: The algorithm and validation. *J. Appl. Meteor.*, **39**, 1248–1268, https://doi.org/10.1175/1520-0450(2000)039<1248:GSOTAF>2.0.CO;2.

Li, Z. L., J. Li, W. P. Menzel, J. P. Nelson III, T. J. Schmit, E. Weisz, and S. A. Ackerman, 2009: Forecasting and nowcasting improvement in cloudy regions with high temporal GOES Sounder infrared radiance measurements. *J. Geophys. Res.*, **114**, D09216, https://doi.org/10.1029/2008JD010596.

Li, J., J. L. Li, J. Otkin, T. J. Schmit, and C.-Y., Liu, 2011: Warning information in a preconvection environment from the geostationary advanced infrared sounding system—a simulation study using the IHOP Case. *Journal of Applied Meteorology and Climatology*, **50**, 776–783, https://doi.org/10.1175/2010JAMC2441.1.

Li, J., P. Wang, H. Han, J. L. Li, and J. Zheng, 2016: On the assimilation of satellite sounder data in cloudy skies in numerical weather prediction models. *Journal of Meteorological Research*, **30**, 169–182, https://doi.org/10.1007/s13351-016-5114-2.

Li, J., Z. L. Li, P. Wang, T. J. Schmit, W. G. Bai, and R. Atlas, 2017: An efficient radiative transfer model for hyperspectral IR radiance simulation and applications under cloudy-sky conditions. *J. Geophys. Res.*, **122**, 7600–7613, https://doi.org/10.1002/2016JD026273.

Lim, A., and Coauthors, 2017: Impact analysis of LEO hyperspectral sensor IFOV size on the next-generation high-resolution NWP model forecast performance. *Proc. 27th International TOVS Study Conf.*, Darmstadt, Germany, NOAA.

Liu, Z.-Q., and F. Rabier, 2002: The interaction between model resolution, observation resolution and observation density in data assimilation: A one-dimensional study. *Quart. J. Roy. Meteor. Soc.*, **128**, 1367–1386, https://doi.org/10.1256/003590002320373337.

Liu, Z. Q., and F. Rabier, 2003: The potential of high-density observations for numerical weather prediction: A study with simulated observations. *Quart. J. Roy. Meteor. Soc.*, **129**, 3013–3035, https://doi.org/10.1256/qj.02.170.

Lynch, P., and X. Y. Huang, 1992: Initialization of the HIRLAM Model using a Digital Filter. *Mon. Wea. Rev.*, **120**, 1019–1034, https://doi.org/10.1175/1520-0493(1992)120<1019:IOTHMU>2.0.CO;2.

Ma, Z. Z., E. S. Maddy, B. L. Zhang, T. Zhu, and S. A. Boukabara, 2017: Impact assessment of *himawari*-8 AHI data assimilation in NCEP GDAS/GFS with GSI. *J. Atmos. Oceanic Technol.*, **34**, 797–815, https://doi.org/10.1175/JTECH-D-16-0136.1.

Mallick, S., D. Dutta, and K.-H. Min, 2017: Quality assessment and forecast sensitivity of global remote sensing observations. *Adv. Atmos.* Sci., **34**(3), 371–382, https://doi.org/10.1007/s00376-016-6109-8.

McNally, A. P., P. D. Watts, J. A. Smith, R. Engelen, G. A. Kelly, J. N. Thépaut, and M. Matricardi, 2006: The assimilation of AIRS radiance data at ECMWF. *Quart. J. Roy. Meteor. Soc.*, **132**, 935–957, https://doi.org/10.1256/qj.04.171.

McNally, A. P., M. Bonavita, and J.-N. Thépaut, 2014: The role of satellite data in the forecasting of hurricane sandy. *Mon. Wea. Rev.*, **142**, 634–646, https://doi.org/10.1175/MWR-D-13-00170.1.

Menzel, W. P., F. C. Holt, T. J. Schmit, R. M. Aune, A. J. Schreiner, G. S. Wade, and D. G. Gray, 1998: Application of *GOES*-8/9 soundings to weather forecasting and nowcasting. *Bull. Amer. Meteor. Soc.*, **79**, 2059–2077, https://doi.org/10.1175/1520-0477(1998)079<2059:AOGSTW>2.0.CO;2.

Menzel, W. P., T. J. Schmit, P. Zhang, and J. Li, 2018: Satellite-based atmospheric infrared sounder development and applications. *Bull. Amer. Meteor. Soc.*, **99**, 583–603, https://doi.org/10.1175/BAMS-D-16-0293.1.

Migliorini, S., 2012: On the equivalence between radiance and retrieval assimilation. *Mon. Wea. Rev.*, **140**, 258–265, https://doi.org/10.1175/MWR-D-10-05047.1.

Peckham, S. E., T. G. Smirnova, S. G. Benjamin, J. M. Brown, and J. S. Kenyon, 2016: Implementation of a digital filter initialization in the WRF model and its application in the Rapid Refresh. *Mon. Wea. Rev.*, **144**, 99–106, https://doi.org/10.1175/MWR-D-15-0219.1.

Schmit, T. J., M. M. Gunshor, W. P. Menzel, J. J. Gurka, J. Li, and A. S. Bachmeier, 2005: Introducing the next-generation ad-

vanced baseline imager on GOES-R. *Bull. Amer. Meteor. Soc*., **86**, 1079–1096, https://doi.org/10.1175/BAMS-86-8-1079.

Schmit, T. J., J. Li, S. A. Ackerman, and J. J. Gurka, 2009: High-spectral-and high-temporal-resolution infrared measurements from geostationary orbit. *J. Atmos. Oceanic Technol*., **26**, 2273–2292, https://doi.org/10.1175/2009JTECHA1248.1.

Schmit, T. J., P. Griffith, M. M. Gunshor, J. M. Daniels, S. J. Goodman, and W. J. Lebair, 2017: A closer look at the ABI on the GOES-R series. *Bull. Amer. Meteor. Soc*., **98**, 681–698, https://doi.org/10.1175/BAMS-D-15-00230.1.

Seemann, S. W., J. Li, W. P. Menzel, and L. E. Gumley, 2003: Operational retrieval of atmospheric temperature, moisture, and ozone from MODIS infrared radiances. *J. Appl. Meteor*., **42**, 1072–1091, https://doi.org/10.1175/1520-0450(2003)042<1072:OROATM>2.0.CO;2.

Seemann, S. W., E. E. Borbas, R. O. Knuteson, G. R. Stephenson, and H.-L. Huang, 2008: Development of a global infrared land surface emissivity database for application to clear sky sounding retrievals from multispectral satellite radiance measurements. *Journal of Applied Meteorology and Climatology*, **47**, 108–123, https://doi.org/10.1175/2007JAMC1590.1.

Skamarock, W. C., and M. L. Weisman, 2009: The impact of positive-definite moisture transport on NWP precipitation forecasts. *Mon. Wea. Rev*., **137**, 488–494, https://doi.org/10.1175/2008MWR2583.1.

Strow, L. L., S. E. Hannon, S. De Souza-Machado, H. Motteler, and D. Tobin, 2003: An overview of the AIRS radiative transfer model. *IEEE Transactions on Geoscience and Remote Sensing*, **41**, 303–313, https://doi.org/10.1109/TGRS.2002.808244.

Wang, H. L., X.-Y. Huang, and Y. S. Chen, 2013: An observing system simulation experiment for the impact of MTG Candidate Infrared Sounding mission on regional forecasts: system development and preliminary results. *ISRN Meteorology*, **2013**, 971501, https://doi.org/10.1155/2013/971501.

Wang, P., J. Li, J. L. Li, Z. L. Li, T. J. Schmit, and W. G. Bai, 2014: Advanced infrared sounder subpixel cloud detection with imagers and its impact on radiance assimilation in NWP. *Geophys. Res. Lett*., **41**, 1773–1780, https://doi.org/10.1002/2013GL059067.

Wang, P., and Coauthors, 2015: Assimilation of thermodynamic information from advanced infrared sounders under partially cloudy skies for regional NWP. *J. Geophys. Res*., **120**, 5469–5484, https://doi.org/10.1002/2014JD022976.

Wang, P., J. Li, Z. L. Li, A. H. N. Lim, J. L. Li, T. J. Schmit, and M. D. Goldberg, 2017: The impact of cross-track infrared sounder (CrIS) cloud - cleared radiances on hurricane Joaquin (2015) and Matthew (2016) Forecasts. *J. Geophys. Res*., **122**, 13 201–13 218, https://doi.org/10.1002/2017JD027515.

Wei, H. L., P. Yang, J. Li, B. A. Baum, H.-L. Huang, S. Platnick, Y. X. Hu, and L. Strow, 2004: Retrieval of semitransparent ice cloud optical thickness from Atmospheric Infrared Sounder (AIRS) measurements. *IEEE Transactions on Geoscience and Remote Sensing*, **42**, 2254–2267, https://doi.org/10.1109/TGRS.2004.833780.

Yang, J., Z. Q. Zhang, C. Y. Wei, F. Lu, and Q. Guo, 2017: Introducing the new generation of Chinese geostationary weather satellites, Fengyun 4. *Bull. Amer. Meteor. Soc*., 1637–1658, https://doi.org/10.1175/BAMS-D-16-0065.1.

Zhang, S. X., Z. X. Pu, D. J. Posselt, and R. Atlas, 2017: Impact of CYGNSS ocean surface wind speeds on numerical simulations of a hurricane in observing system simulation experiments. *J. Atmos. Oceanic Technol*., **34**, 375–383, https://doi.org/10.1175/JTECH-D-16-0144.1.

Zhu, Y. Q., J. Derber, A. Collard, D. Dee, R. Treadon, G. Gayno, and J. A. Jung, 2014: Enhanced radiance bias correction in the National Centers for Environmental Prediction's Gridpoint Statistical Interpolation data assimilation system. *Quart. J. Roy. Meteor. Soc*., **140**(682), 1479–1492, https://doi.org/10.1002/qj.2233.